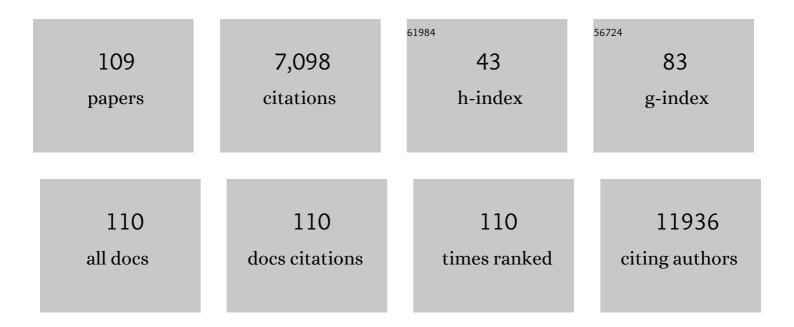
## A T Charlie Johnson

List of Publications by Year in descending order

Source: https://exaly.com/author-pdf/4982094/publications.pdf Version: 2024-02-01



#	Article	IF	CITATIONS
1	Gigahertz topological valley Hall effect in nanoelectromechanical phononic crystals. Nature Electronics, 2022, 5, 157-163.	26.0	37
2	Multimodal, Multiscale Insights into Hippocampal Seizures Enabled by Transparent, Graphene-Based Microelectrode Arrays. ENeuro, 2022, 9, ENEURO.0386-21.2022.	1.9	2
3	Temperature dependent charge transport in ferroelectrically gated graphene far from the Dirac point. AIP Advances, 2022, 12, 075008.	1.3	1
4	Multimodal in vivo recording using transparent graphene microelectrodes illuminates spatiotemporal seizure dynamics at the microscale. Communications Biology, 2021, 4, 136.	4.4	28
5	The C-Terminus of the mu Opioid Receptor Is Critical in G-Protein Interaction as Demonstrated by a Novel Graphene Biosensor. IEEE Sensors Journal, 2021, 21, 5758-5762.	4.7	0
6	Scalable chemical vapor deposited graphene field-effect transistors for bio/chemical assay. Applied Physics Reviews, 2021, 8, .	11.3	10
7	Rapid Growth of Monolayer MoSe <sub>2</sub> Films for Largeâ€Area Electronics. Advanced Electronic Materials, 2021, 7, 2001219.	5.1	14
8	Impurity charge compensation in graphene by a polarized ferroelectric polymer and its effect on charge transport near the Dirac point. AIP Advances, 2021, 11, .	1.3	1
9	Quantum-Well Bound States in Graphene Heterostructure Interfaces. Physical Review Letters, 2021, 127, 086805.	7.8	5
10	Azimuthally Polarized and Unidirectional Excitonic Emission from Deep Subwavelength Transition Metal Dichalcogenide Annular Heterostructures. ACS Photonics, 2021, 8, 2861-2867.	6.6	3
11	Multi-order phononic frequency comb generation within a MoS2 electromechanical resonator. Applied Physics Letters, 2021, 119, .	3.3	6
12	Strain and Spin-Orbit Coupling Engineering in Twisted WS2/Graphene Heterobilayer. Nanomaterials, 2021, 11, 2921.	4.1	10
13	Characterization of an engineered water-soluble variant of the full-length human mu opioid receptor. Journal of Biomolecular Structure and Dynamics, 2020, 38, 4364-4370.	3.5	4
14	Graphene transistor arrays functionalized with genetically engineered antibody fragments for Lyme disease diagnosis. 2D Materials, 2020, 7, 024001.	4.4	19
15	MoS <sub>2</sub> -enabled dual-mode optoelectronic biosensor using a water soluble variant of µ-opioid receptor for opioid peptide detection. 2D Materials, 2020, 7, 014004.	4.4	15
16	Phase Transition in a Memristive Suspended MoS <sub>2</sub> Monolayer Probed by Opto- and Electro-Mechanics. ACS Nano, 2020, 14, 13611-13618.	14.6	13
17	Exploring ovarian cancer screening using a combined sensor approach: A pilot study. AIP Advances, 2020, 10, .	1.3	13
18	Nanoscale Friction Behavior of Transition-Metal Dichalcogenides: Role of the Chalcogenide. ACS Nano, 2020, 14, 16013-16021.	14.6	36

#	Article	IF	CITATIONS
19	Controlled doping of graphene by impurity charge compensation via a polarized ferroelectric polymer. Journal of Applied Physics, 2020, 127, .	2.5	6
20	Attomolar Detection of ssDNA Without Amplification and Capture of Long Target Sequences With Graphene Biosensors. IEEE Sensors Journal, 2020, 20, 5720-5724.	4.7	14
21	Large-area epitaxial growth of curvature-stabilized ABC trilayer graphene. Nature Communications, 2020, 11, 546.	12.8	47
22	Ultrathin WS <sub>2</sub> â€onâ€Glass Photonic Crystal for Selfâ€Resonant Excitonâ€Polaritonics. Advanced Optical Materials, 2020, 8, 1901988.	7.3	14
23	Ionic liquid gel gate tunable p-Si/MoS2 heterojunction p-n diode. AIP Advances, 2020, 10, 125225.	1.3	3
24	Recentadvances in the propertiesand synthesis of bilayer graphene and transition metal dichalcogenides. JPhys Materials, 2020, 3, 042003.	4.2	11
25	Controlled Growth of Large-Area Bilayer Tungsten Diselenides with Lateral P–N Junctions. ACS Nano, 2019, 13, 10490-10498.	14.6	39
26	Monolayer Excitonic Emission for Imaging Spatial Dispersion of Photonic Crystals. ACS Photonics, 2019, 6, 2312-2319.	6.6	7
27	Origin of Nanoscale Friction Contrast between Supported Graphene, MoS <sub>2</sub> , and a Graphene/MoS <sub>2</sub> Heterostructure. Nano Letters, 2019, 19, 5496-5505.	9.1	115
28	Rectifying effect in a MoS2 monolayer crossed with an electro-spun PEDOT-PSS nano-ribbon. SN Applied Sciences, 2019, 1, 1.	2.9	1
29	Atomic-scale patterning in two-dimensional van der waals superlattices. Nanotechnology, 2019, 31, 105302.	2.6	8
30	Loss and coupling tuning via heterogeneous integration of MoS2 layers in silicon photonics [Invited]. Optical Materials Express, 2019, 9, 751.	3.0	32
31	Scalable Arrays of Chemical Vapor Sensors Based on DNA-Decorated Graphene. Methods in Molecular Biology, 2019, 2027, 163-170.	0.9	2
32	Water Soluble G-protein Coupled Receptor Enabled Biosensors. Translational Perioperative and Pain Medicine, 2019, 6, 98-103.	0.1	4
33	Crystalline Bilayer Graphene with Preferential Stacking from Ni–Cu Gradient Alloy. ACS Nano, 2018, 12, 2275-2282.	14.6	43
34	All-Electronic Quantification of Neuropeptide–Receptor Interaction Using a Bias-Free Functionalized Graphene Microelectrode. ACS Nano, 2018, 12, 4218-4223.	14.6	13
35	Dynamic Photochemical and Optoelectronic Control of Photonic Fano Resonances via Monolayer MoS <sub>2</sub> Trions. Nano Letters, 2018, 18, 957-963.	9.1	31
36	Intrinsic Properties of Suspended MoS <sub>2</sub> on SiO <sub>2</sub> /Si Pillar Arrays for Nanomechanics and Optics. ACS Nano, 2018, 12, 3235-3242.	14.6	62

#	Article	IF	CITATIONS
37	Understanding the Different Exciton–Plasmon Coupling Regimes in Two-Dimensional Semiconductors Coupled with Plasmonic Lattices: A Combined Experimental and Unified Equation of Motion Approach. ACS Photonics, 2018, 5, 192-204.	6.6	30
38	Highly active single-layer MoS <sub>2</sub> catalysts synthesized by swift heavy ion irradiation. Nanoscale, 2018, 10, 22908-22916.	5.6	39
39	Detection of Sub-fM DNA with Target Recycling and Self-Assembly Amplification on Graphene Field-Effect Biosensors. Nano Letters, 2018, 18, 3509-3515.	9.1	82
40	DNA Nanotweezers and Graphene Transistor Enable Labelâ€Free Genotyping. Advanced Materials, 2018, 30, e1802440.	21.0	73
41	Ambipolar transport in CVD grown MoSe2 monolayer using an ionic liquid gel gate dielectric. AIP Advances, 2018, 8, .	1.3	14
42	Quantifying the effect of ionic screening with protein-decorated graphene transistors. Biosensors and Bioelectronics, 2017, 89, 689-692.	10.1	35
43	Defect engineering of single- and few-layer MoS <sub>2</sub> by swift heavy ion irradiation. 2D Materials, 2017, 4, 015034.	4.4	60
44	Tunable Doping in Hydrogenated Single Layered Molybdenum Disulfide. ACS Nano, 2017, 11, 1755-1761.	14.6	86
45	Monolayer WS <sub>2</sub> Nanopores for DNA Translocation with Light-Adjustable Sizes. ACS Nano, 2017, 11, 1937-1945.	14.6	102
46	Transfer of monolayer TMD WS2 and Raman study of substrate effects. Scientific Reports, 2017, 7, 43037.	3.3	51
47	Large-area synthesis of high-quality monolayer 1T'-WTe <sub>2</sub> flakes. 2D Materials, 2017, 4, 021008.	4.4	81
48	Inverting polar domains via electrical pulsing in metallic germanium telluride. Nature Communications, 2017, 8, 15033.	12.8	29
49	Ambient effects on electrical characteristics of CVD-grown monolayer MoS2 field-effect transistors. Scientific Reports, 2017, 7, 4075.	3.3	57
50	Structural-functional analysis of engineered protein-nanoparticle assemblies using graphene microelectrodes. Chemical Science, 2017, 8, 5329-5334.	7.4	4
51	pH Sensing Properties of Flexible, Biasâ€Free Graphene Microelectrodes in Complex Fluids: From Phosphate Buffer Solution to Human Serum. Small, 2017, 13, 1700564.	10.0	5
52	Electrical Tuning of Exciton–Plasmon Polariton Coupling in Monolayer MoS <sub>2</sub> Integrated with Plasmonic Nanoantenna Lattice. Nano Letters, 2017, 17, 4541-4547.	9.1	117
53	Intrinsic Phonon Bands in High-Quality Monolayer <i>T</i> ′ Molybdenum Ditelluride. ACS Nano, 2017, 11, 814-820. Interface dipole and band bending in the hybrid <mml:math< td=""><td>14.6</td><td>37</td></mml:math<>	14.6	37
54	xmlns:mml="http://www.w3.org/1998/Math/MathML"> <mml:mrow> <mml:mi>p</mml:mi> <mml:mo>â<sup>~</sup> heterojunction <mml:math xmlns:mml="http://www.w3.org/1998/Math/MathML"&gt; <mml:mrow> <mml:mi> Mo</mml:mi> <mml:msub> <mml mathvariant="normal"&gt;S  <mml:mn>2 </mml:mn> </mml </mml:msub> <mml:mo>/</mml:mo> <mml:mi>GaN &lt; Physical Review B, 2017, 96, .</mml:mi></mml:mrow></mml:math </mml:mo></mml:mrow>	:mi <sup>3.2</sup>	57

#	Article	IF	CITATIONS
55	Unidirectional Doubly Enhanced MoS <sub>2</sub> Emission via Photonic Fano Resonances. Nano Letters, 2017, 17, 6715-6720.	9.1	69
56	Synthesis and Physical Properties of Phase-Engineered Transition Metal Dichalcogenide Monolayer Heterostructures. ACS Nano, 2017, 11, 8619-8627.	14.6	42
57	Scalable graphene aptasensors for drug quantification. AIP Advances, 2017, 7, .	1.3	16
58	An Aptamer-Based Biosensor for the Azole Class of Antifungal Drugs. MSphere, 2017, 2, .	2.9	18
59	MoS2 based dual input logic AND gate. AIP Advances, 2016, 6, 125041.	1.3	4
60	Electrolytic phototransistor based on graphene-MoS2 van der Waals p-n heterojunction with tunable photoresponse. Applied Physics Letters, 2016, 109, .	3.3	41
61	Quantifying the intrinsic surface charge density and charge-transfer resistance of the graphene-solution interface through bias-free low-level charge measurement. Applied Physics Letters, 2016, 109, .	3.3	14
62	Photothermal characterization of MoS2 emission coupled to a microdisk cavity. Applied Physics Letters, 2016, 109, .	3.3	13
63	Scalable Production of Molybdenum Disulfide Based Biosensors. ACS Nano, 2016, 10, 6173-6179.	14.6	68
64	Monolayer Single-Crystal 1T′-MoTe <sub>2</sub> Grown by Chemical Vapor Deposition Exhibits Weak Antilocalization Effect. Nano Letters, 2016, 16, 4297-4304.	9.1	205
65	Scalable Production of Sensor Arrays Based on High-Mobility Hybrid Graphene Field Effect Transistors. ACS Applied Materials & Interfaces, 2016, 8, 27546-27552.	8.0	44
66	Scalable Production of High-Sensitivity, Label-Free DNA Biosensors Based on Back-Gated Graphene Field Effect Transistors. ACS Nano, 2016, 10, 8700-8704.	14.6	145
67	Large area molybdenum disulphide- epitaxial graphene vertical Van der Waals heterostructures. Scientific Reports, 2016, 6, 26656.	3.3	73
68	Band Alignment and Minigaps in Monolayer MoS <sub>2</sub> -Graphene van der Waals Heterostructures. Nano Letters, 2016, 16, 4054-4061.	9.1	288
69	Strong Exciton–Plasmon Coupling in MoS <sub>2</sub> Coupled with Plasmonic Lattice. Nano Letters, 2016, 16, 1262-1269.	9.1	331
70	Raman Shifts in Electron-Irradiated Monolayer MoS <sub>2</sub> . ACS Nano, 2016, 10, 4134-4142.	14.6	311
71	Observing Oxygen Vacancy Driven Electroforming in Pt–TiO <sub>2</sub> –Pt Device via Strong Metal Support Interaction. Nano Letters, 2016, 16, 2139-2144.	9.1	73
72	<i>In Situ</i> Transmission Electron Microscopy Modulation of Transport in Graphene Nanoribbons. ACS Nano, 2016, 10, 4004-4010.	14.6	33

#	Article	IF	CITATIONS
73	Optomechanical Enhancement of Doubly Resonant 2D Optical Nonlinearity. Nano Letters, 2016, 16, 1631-1636.	9.1	71
74	Effect of conductive additives to gel electrolytes on activated carbon-based supercapacitors. AIP Advances, 2015, 5, .	1.3	42
75	Fabrication and Simultaneous Electrical Measurement of Graphene Nanoribbon Devices Inside a S/TEM. Microscopy and Microanalysis, 2015, 21, 1155-1156.	0.4	0
76	Electronic Transport of Recrystallized Freestanding Graphene Nanoribbons. ACS Nano, 2015, 9, 3510-3520.	14.6	44
77	Seeded growth of highly crystalline molybdenum disulphide monolayers at controlled locations. Nature Communications, 2015, 6, 6128.	12.8	259
78	Fano Resonance and Spectrally Modified Photoluminescence Enhancement in Monolayer MoS <sub>2</sub> Integrated with Plasmonic Nanoantenna Array. Nano Letters, 2015, 15, 3646-3653.	9.1	246
79	Facile fabrication of a ultraviolet tunable MoS2/ <i>p</i> -Si junction diode. Applied Physics Letters, 2015, 106, .	3.3	21
80	Electronic Transport in Heterostructures of Chemical Vapor Deposited Graphene and Hexagonal Boron Nitride. Small, 2015, 11, 1402-1408.	10.0	14
81	Scalable Production of Highly Sensitive Nanosensors Based on Graphene Functionalized with a Designed G Protein-Coupled Receptor. Nano Letters, 2014, 14, 2709-2714.	9.1	105
82	Scalable arrays of chemical vapor sensors based on DNA-decorated graphene. Nano Research, 2014, 7, 95-103.	10.4	45
83	Frictional Behavior of Atomically Thin Sheets: Hexagonal-Shaped Graphene Islands Grown on Copper by Chemical Vapor Deposition. ACS Nano, 2014, 8, 5010-5021.	14.6	136
84	Solvothermal synthesis of NiAl double hydroxide microspheres on a nickel foam-graphene as an electrode material for pseudo-capacitors. AIP Advances, 2014, 4, 097122.	1.3	13
85	Correlating Atomic Structure and Transport in Suspended Graphene Nanoribbons. Nano Letters, 2014, 14, 4238-4244.	9.1	71
86	Characterization of a Computationally Designed Water-soluble Human μ-Opioid Receptor Variant Using Available Structural Information. Anesthesiology, 2014, 121, 866-875.	2.5	13
87	Scalable, non-invasive glucose sensor based on boronic acid functionalized carbon nanotube transistors. Applied Physics Letters, 2013, 102, .	3.3	73
88	DNA-decorated graphene nanomesh for detection of chemical vapors. Applied Physics Letters, 2013, 103, 183110.	3.3	45
89	High-performance symmetric electrochemical capacitor based on graphene foam and nanostructured manganese oxide. AIP Advances, 2013, 3, .	1.3	86
90	Growth of graphene underlayers by chemical vapor deposition. AIP Advances, 2013, 3, .	1.3	13

#	Article	IF	CITATIONS
91	Differentiation of Complex Vapor Mixtures Using Versatile DNA–Carbon Nanotube Chemical Sensor Arrays. ACS Nano, 2013, 7, 2800-2807.	14.6	71
92	Graphene-protein bioelectronic devices with wavelength-dependent photoresponse. Applied Physics Letters, 2012, 100, .	3.3	41
93	Controlled doping of graphene using ultraviolet irradiation. Applied Physics Letters, 2012, 100, 253108.	3.3	94
94	Toward Quantifying the Electrostatic Transduction Mechanism in Carbon Nanotube Molecular Sensors. Journal of the American Chemical Society, 2012, 134, 14318-14321.	13.7	48
95	Effect of Substrate Roughness and Feedstock Concentration on Growth of Wafer-Scale Graphene at Atmospheric Pressure. Chemistry of Materials, 2011, 23, 1441-1447.	6.7	277
96	Growth Mechanism of Hexagonal-Shape Graphene Flakes with Zigzag Edges. ACS Nano, 2011, 5, 9154-9160.	14.6	154
97	Editorial: Welcome to AIP Advances—a new open-access journal from the American Institute of Physics. AIP Advances, 2011, 1, 010401.	1.3	0
98	A carbon nanotube immunosensor for <i>Salmonella</i> . AIP Advances, 2011, 1, .	1.3	29
99	High-Throughput Nanogap Formation Using Single Ramp Feedback Control. IEEE Nanotechnology Magazine, 2011, 10, 806-809.	2.0	6
100	Highâ€On/Offâ€Ratio Graphene Nanoconstriction Fieldâ€Effect Transistor. Small, 2010, 6, 2748-2754.	10.0	80
101	The Nature of DNAâ€Base–Carbonâ€Nanotube Interactions. Small, 2010, 6, 31-34.	10.0	108
102	DNA-Coated Nanosensors for Breath Analysis. IEEE Sensors Journal, 2010, 10, 159-166.	4.7	27
103	DNA Translocation through Graphene Nanopores. Nano Letters, 2010, 10, 2915-2921.	9.1	846
104	Structural and magnetic properties of ε-Fe1â^'xCoxSi thin films deposited via pulsed laser deposition. Applied Physics Letters, 2009, 94, 232503.	3.3	9
105	Photoluminescence and band gap modulation in graphene oxide. Applied Physics Letters, 2009, 94, .	3.3	494
106	Real-Time TEM Imaging of the Formation of Crystalline Nanoscale Gaps. Physical Review Letters, 2008, 100, 056805.	7.8	77
107	Gas Phase Electronic Sensing Using Single Wall Carbon Nanotube/Boipolymer Hybrids. Materials Research Society Symposia Proceedings, 2007, 1057, 1.	0.1	0
108	Effect of Thermal Treatments on the Transduction Behaviors of Conductometric Hydrogen Gas Sensors Integrated with HCl-Doped Polyaniline Nanofibers. Materials Research Society Symposia Proceedings, 2007, 1042, 1.	0.1	0

#	Article	IF	CITATIONS
109	DNA-decorated carbon nanotubes for chemical sensing. Physica Status Solidi (B): Basic Research, 2006, 243, 3252-3256.	1.5	24